Synthesis design of interfacial structure for highly reversible lithium deposition

Shuwei Wang[1 a,b], Lihan Zhang[1 a,b], Xingke Cai[c], Tianzhi Chu[c], Dongqing Liu[d], Cuiping Han[a], Xianying Qin[a*], Feiyu Kang [a], Baohua Li[a*]

a Shenzhen Key Laboratory on Power Battery Safety Research and Shenzhen Geim Graphene Center, Tsinghua Shenzhen International Graduate School, Shenzhen 518055, China

b Laboratory of Advanced Materials, School of Materials Science and Engineering, Tsinghua University, Beijing 100084, China

c Institute for Advanced Study, Shenzhen University, Shenzhen, 518060 China

d Shenzhen Key Laboratory of High Performance Nontraditional Manufacturing, College of Mechatronics and Control Engineering, Shenzhen University, Shenzhen, 518060, China

*Email: libh@mail.sz.tsinghua.edu.cn (Baohua Li)

*Email: qinxianying2005@126.com (Xianying Qin)

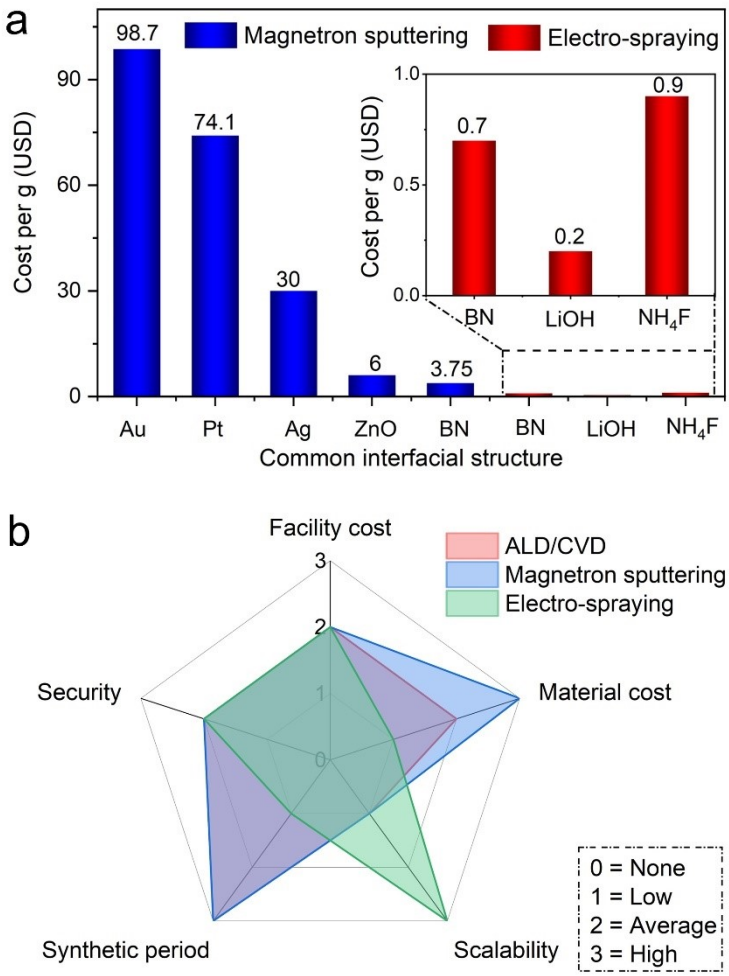

Figure S1. (a) Estimated unit prices of different raw materials of common interfacial structure used in magnetron sputtering and electro-spraying process. (b) Main properties of commonly adopted methods to synthesize interfacial structure.

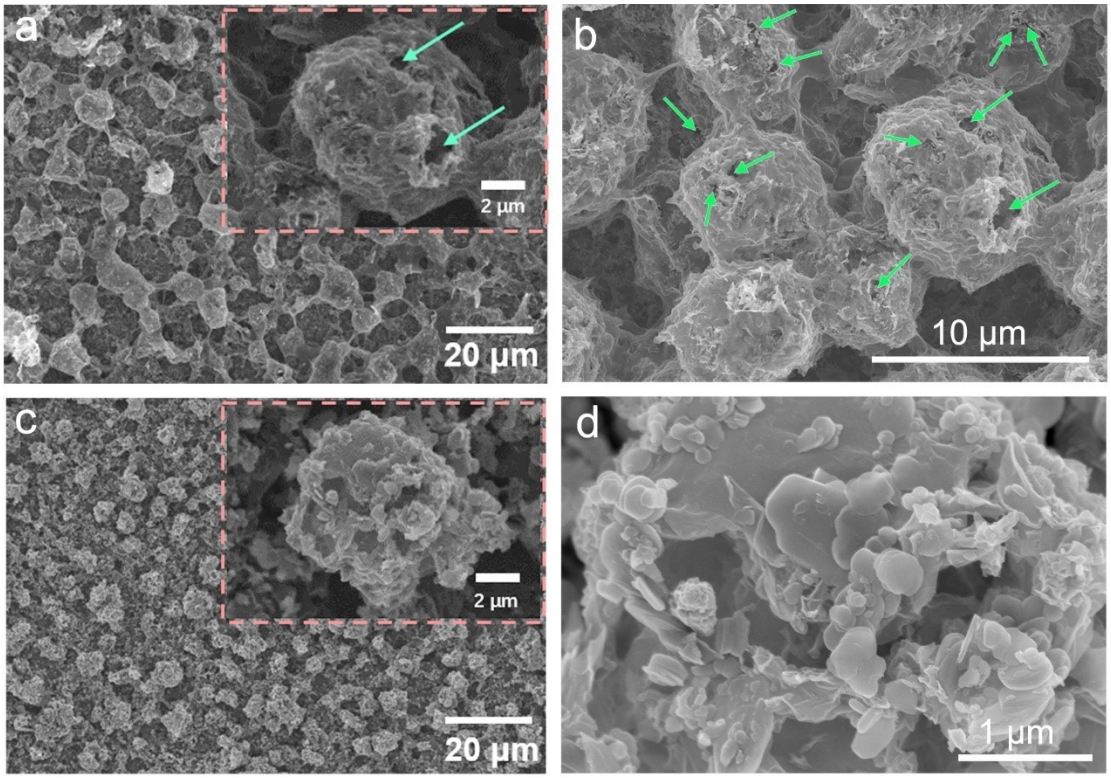

Figure S2. (a,b) SEM images of 3D rGO skeleton. (c,d) SEM images of 3D BIG host.

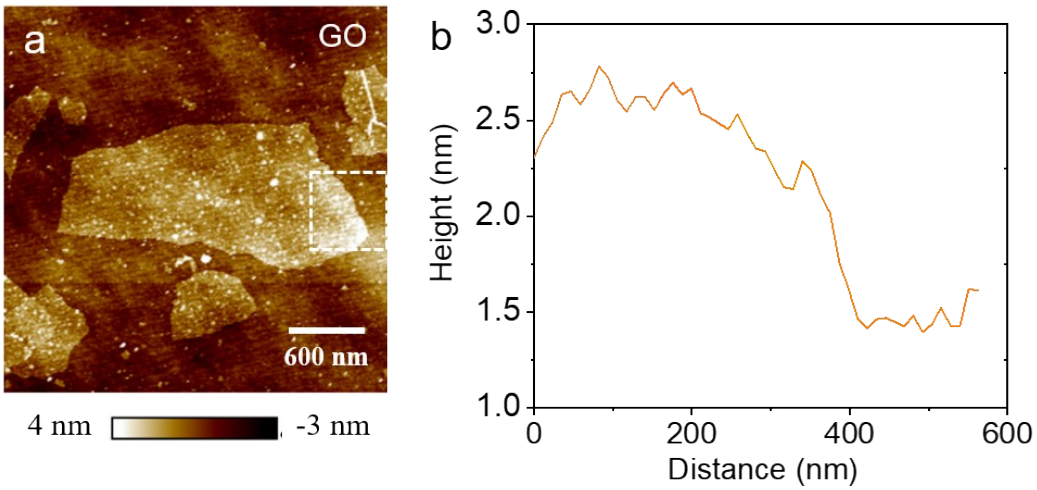

Figure S3. AFM images of bare graphene (a) and height profile of single layer GO flake (b) on Si substrate.

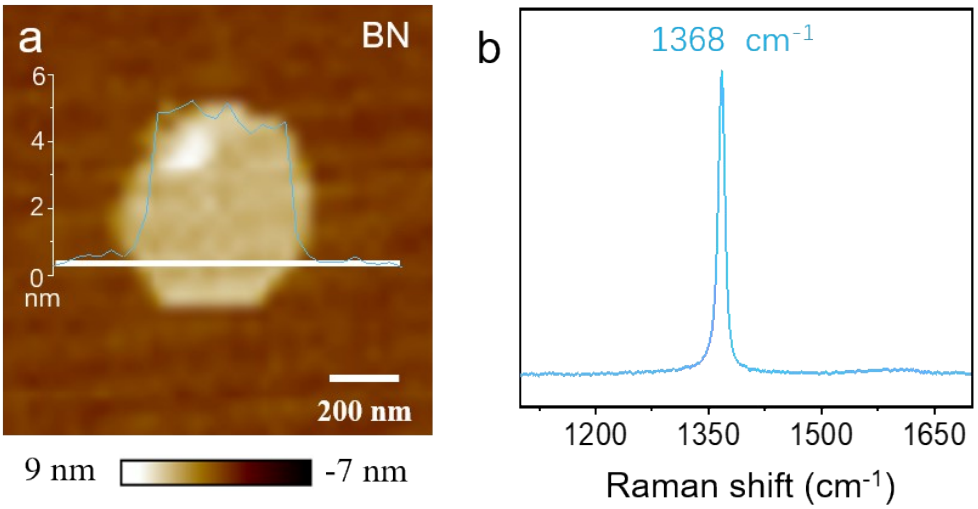

Figure S4. (a) AFM images of BN nanosheet. (b) Raman spectrum of few layered h-BN film on Si.

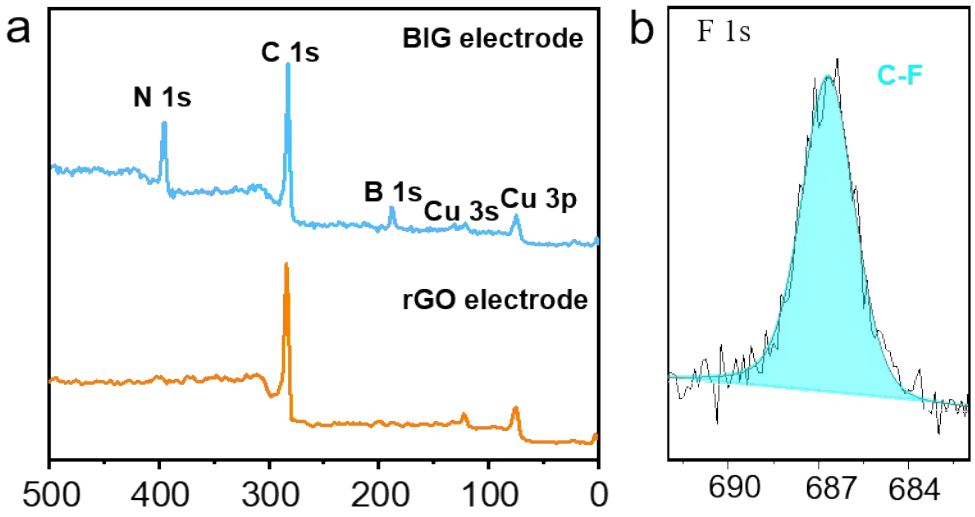

Figure S5. (a) Full XPS spectrum of 3D rGO and BIG electrodes indicating the part of existence elements. (b) XPS spectra of F 1s of 3D BIG electrode.

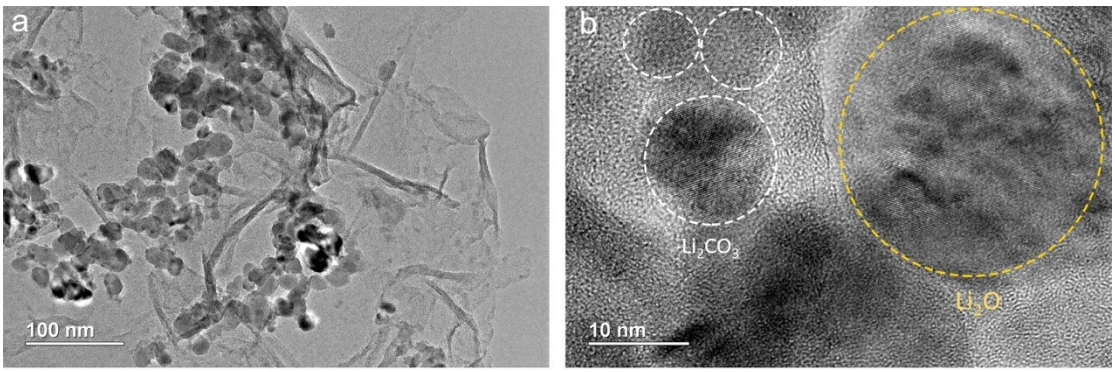

Figure S6. (a) TEM image of inorganic particles dispersed on rGO layers. (b) HRTEM image of inorganic particle.

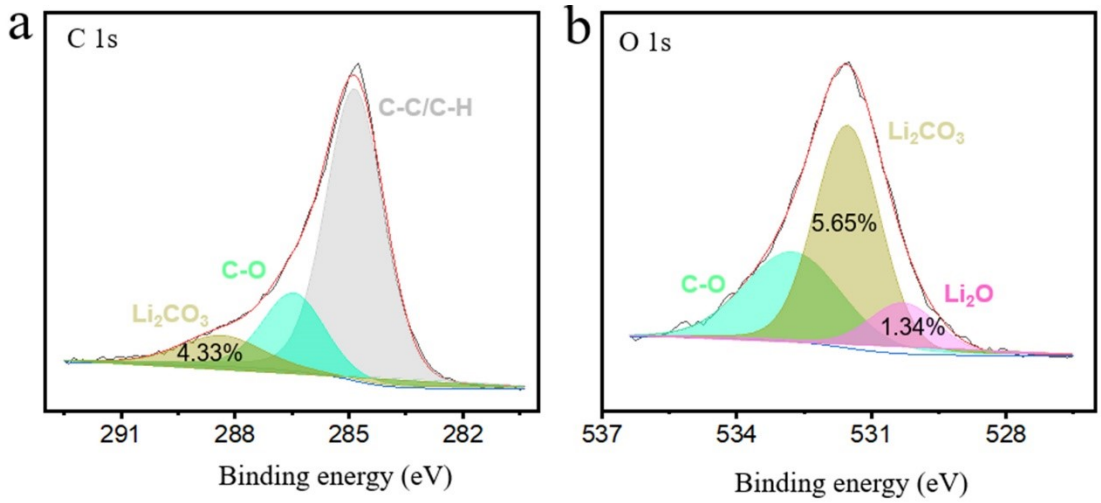

Figure S7. (a) C1s and O1s (b) XPS spectra of the BIG skeleton.

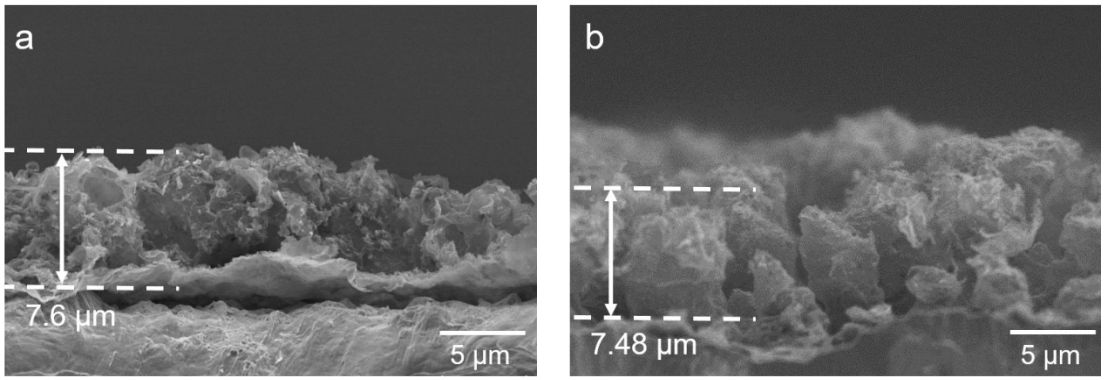

Figure S8. Cross-sectional view SEM images of the BIG (a) and rGO (b) host, respectively.

Figure S9. Photographs of a BIG electrode containing Cu substrate (a), the BIG electrode under bending (b) and after bending (c).

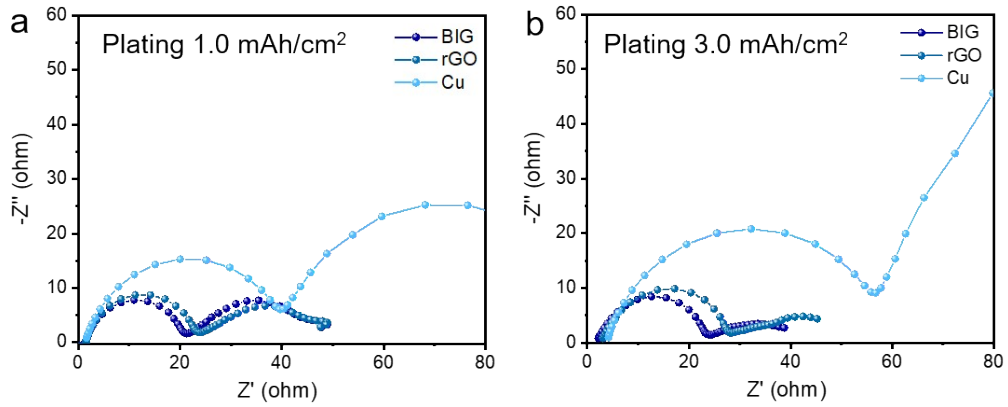

Figure S10. Nyquist plots of three styles of electrodes for plating 1.0 mAh/cm^2 (a) and 3.0 mAh/cm^2 (b).

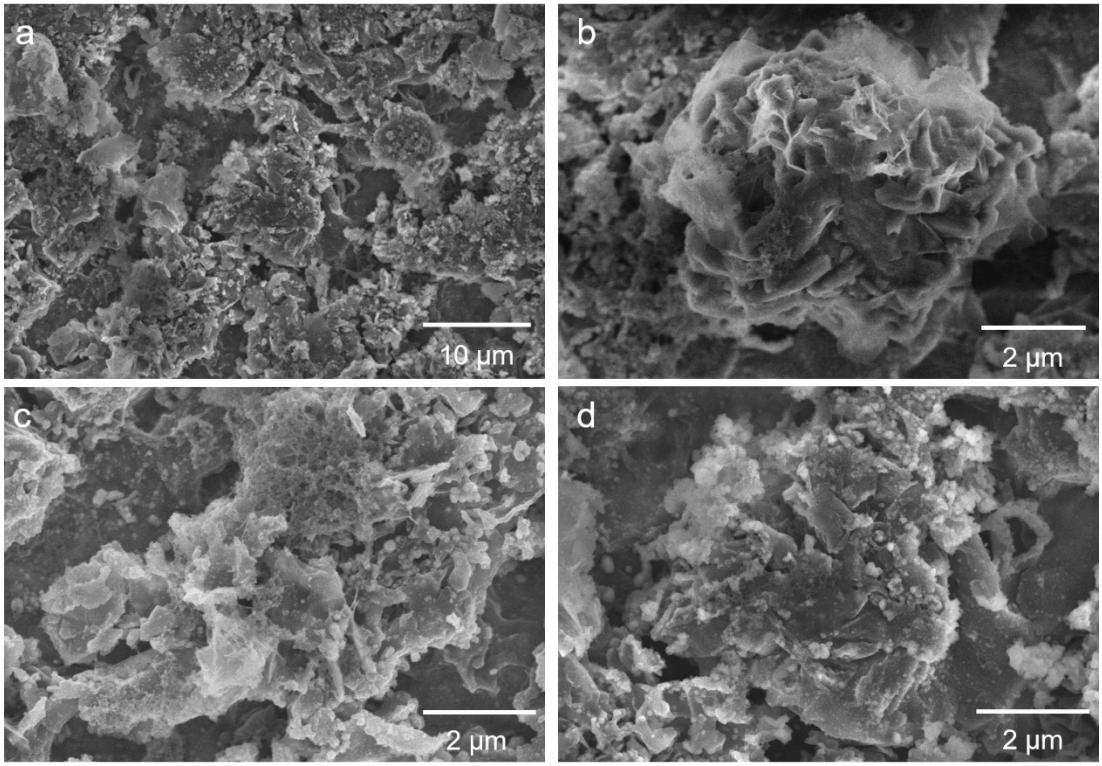

Figure S11. (a) Low- magnification and high- magnification (b-d) SEM images of rGO skeleton after plating 0.1 mA h/cm^2 Li at different regions.

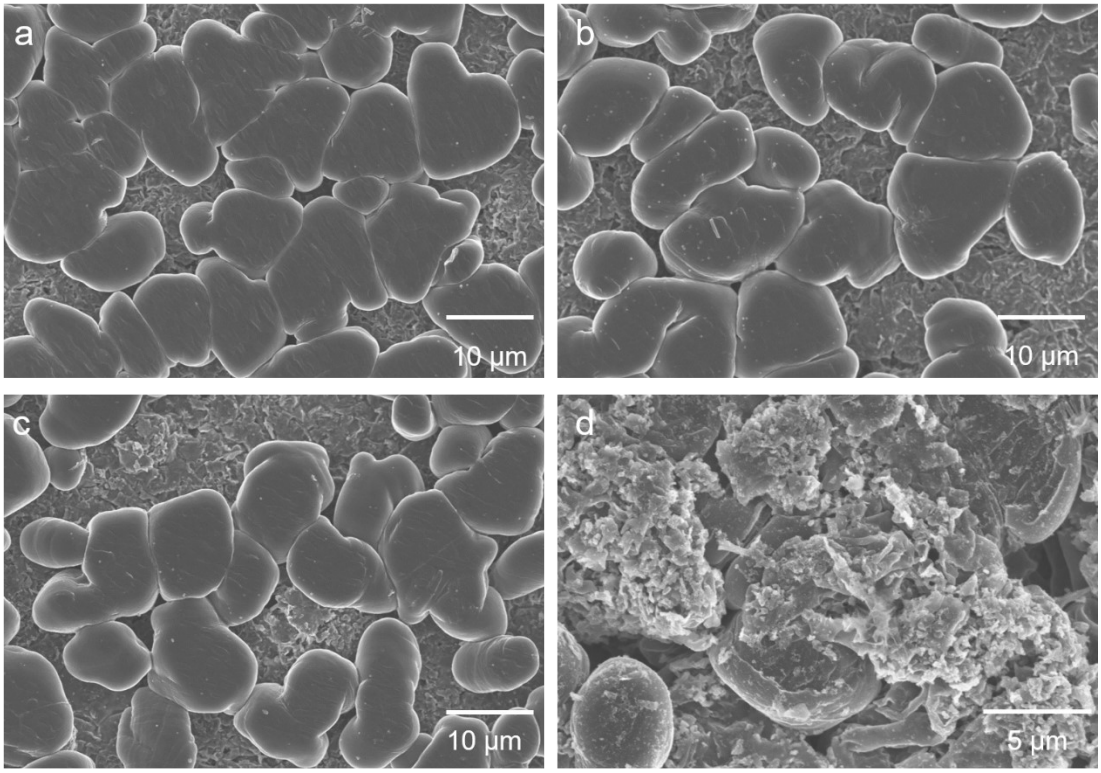

Figure S12. (a-d) SEM images of rGO skeleton after plating 1 mA h/cm^2 Li at different regions.

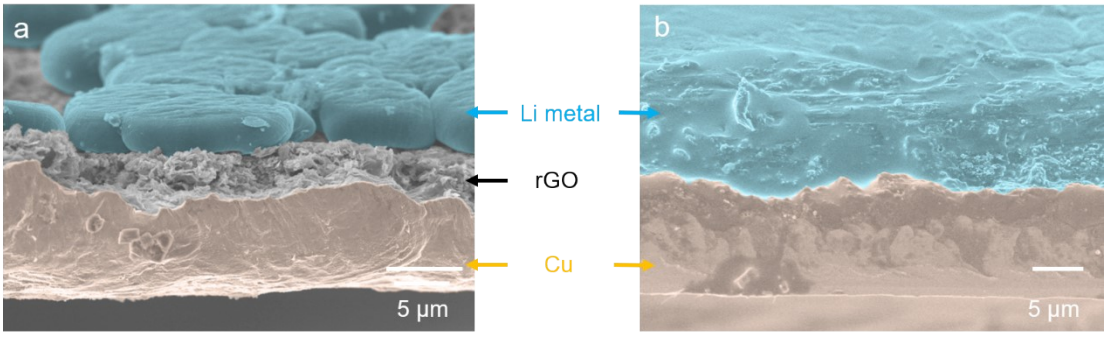

Figure S13. Cross-section SEM images of 3D rGO (a) and BIG (b) electrodes with 1.0 mAh/cm^2 Li deposition.

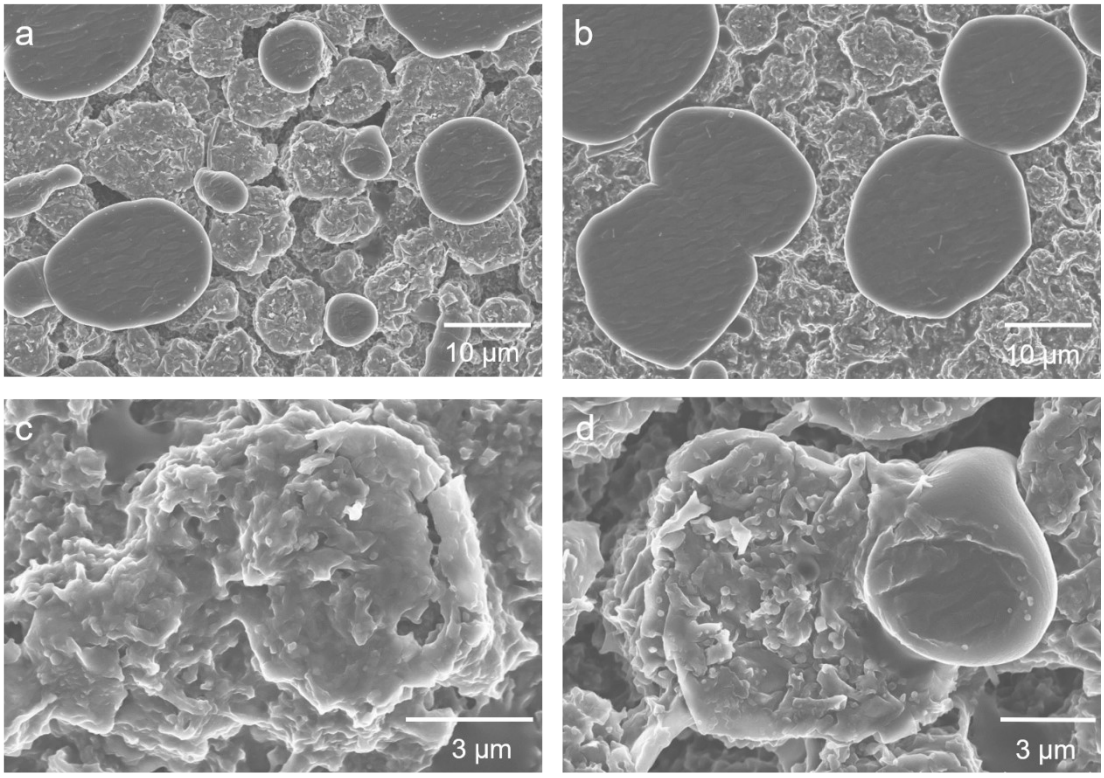

Figure S14. (a,b) Low- magnification and high- magnification (c,d) SEM images of rGO skeleton after stripping at different regions.

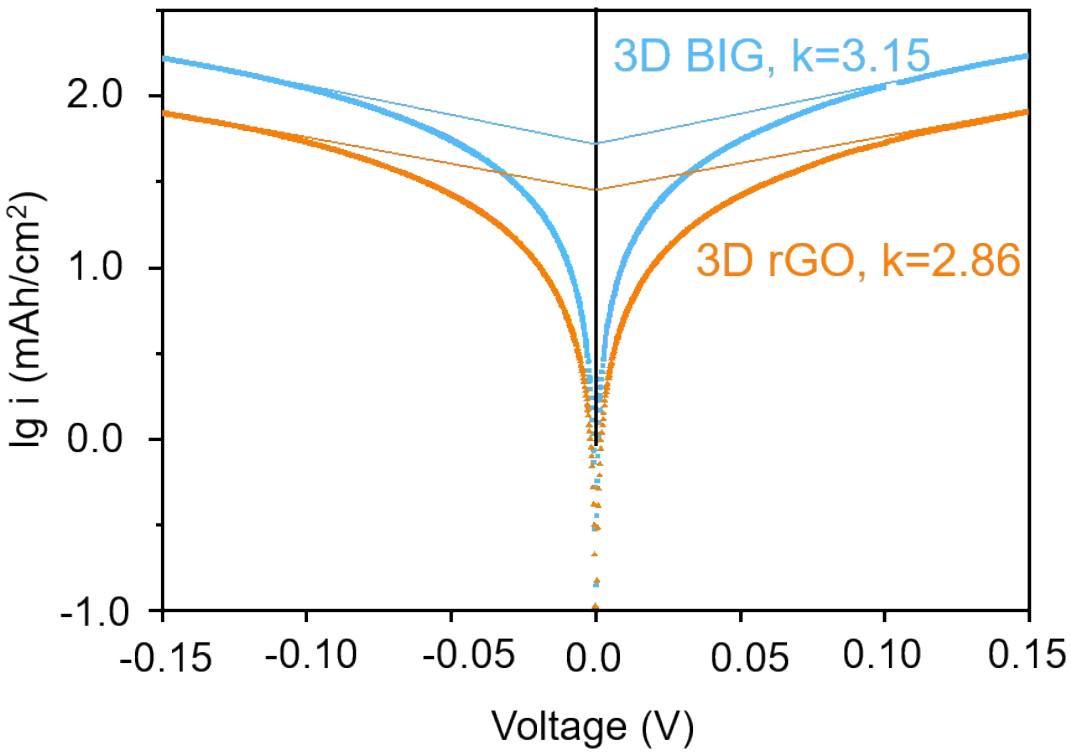

Figure S15. Tafel plots of 3D rGO and BIG electrodes.

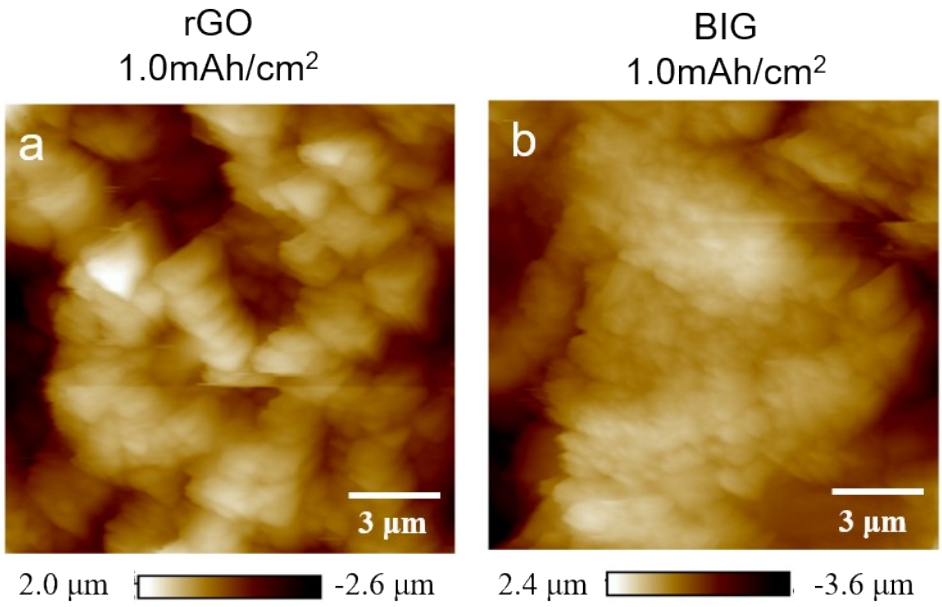

Figure S16. The topological images corresponding to Figure 6(a, b).

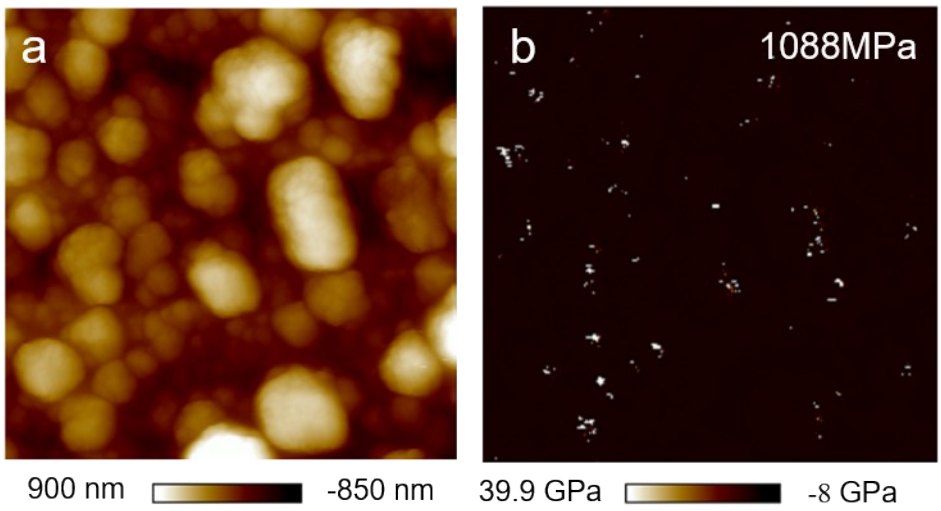

Figure S17. The topological images of the SEI layer formed on Cu electrode after plating 1.0 mAh/cm^2 and corresponding modulus distribution of the SEI layer.

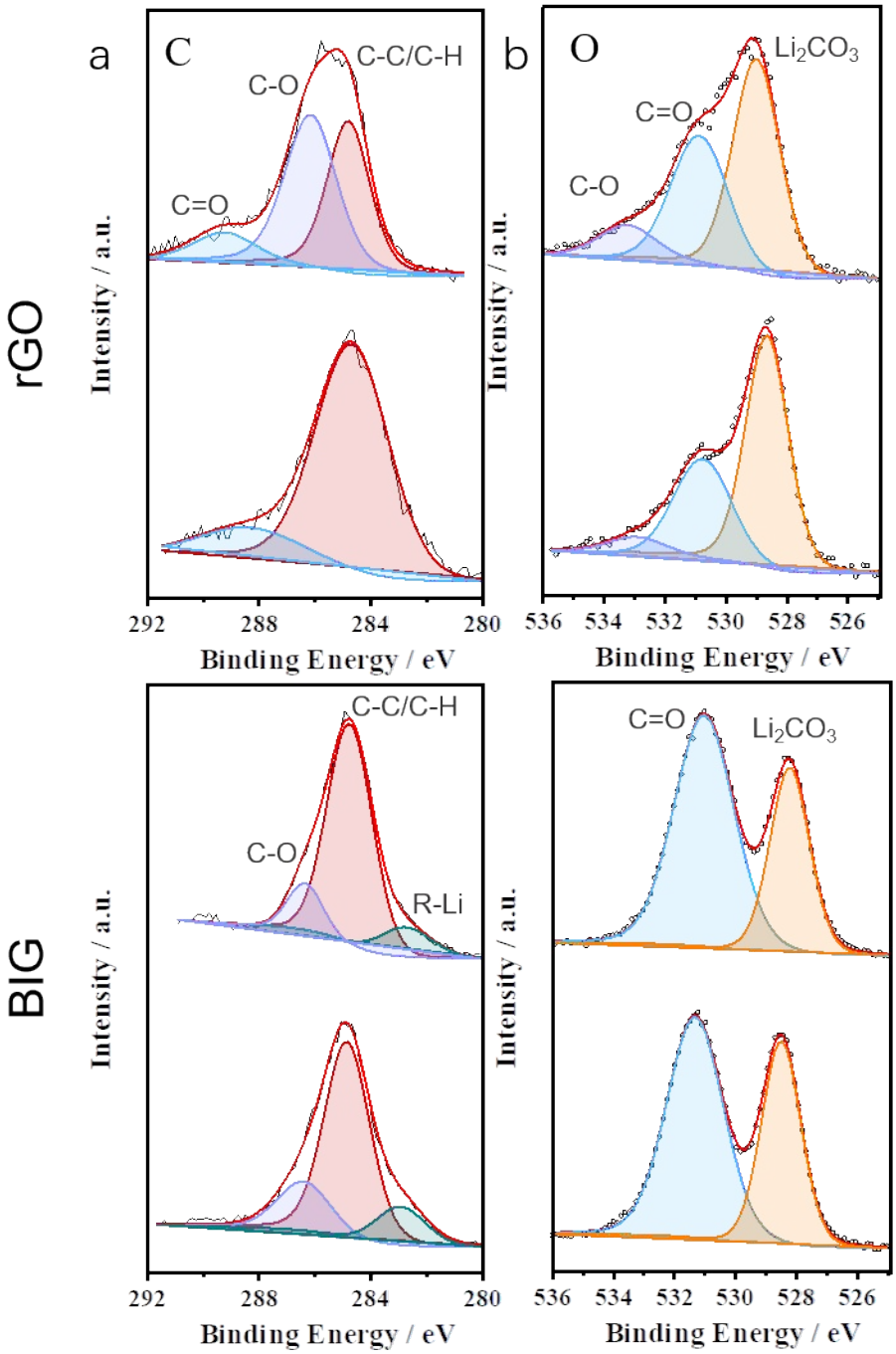

Figure S18. The composition of the SEI layer after deposition capacity of 1.0 mAh/cm^2 on 3D rGO and BIG electrodes. (a) C 1s and (b) O 1s.